Received: 15 April 2022 | Revised: 26 June 2022 | Accepted: 14 September 2022

DOI: 10.1002/suco.202200373

ARTICLE

fib CEB-FIP WILEY

Time-dependent seismic fragility curves for existing RC core-wall buildings exposed to corrosion

Elena Michelini[1] | **Beatrice Belletti**[1] | **Lorenzo Franceschini**[1] | **Enzo Martinelli**[2]

[1]Department of Engineering and Architecture, University of Parma, Parma, Italy

[2]Department of Civil Engineering, University of Salerno, Fisciano, Italy

Correspondence
Elena Michelini, Department of Engineering and Architecture, University of Parma, Parco Area Delle Scienze 181/A, 43124 Parma, Italy.
Email: elena.michelini@unipr.it

Abstract

This work aims at investigating the seismic response of existing reinforced concrete core-wall buildings with corroded bars erected in the marine environments, with the main focus on the dependency of seismic fragility curves on aging and degradation effects caused by environmental actions. The structural capacity is predicted by nonlinear finite-element analyses, where the effect of chloride corrosion is implemented within the framework of PARC_CL_2.1 crack model. The proposed methodology is applied to a pre-code six-story reinforced concrete (RC) building with moment-resisting (MR) frames and an internal core assumed as a testbed. For a given exposure class, pushover analyses are performed for different ages of the building. Time-dependent fragility curves are then obtained through a procedure based on incremental static analysis. Different corrosion scenarios are assessed by considering deterioration effects applied either on the sole RC walls or on both walls and columns. The obtained results highlight that time-dependent fragility curves are strongly affected by corrosion, therefore the date of construction should be considered in seismic risk mapping, not only for evaluating the effect of obsolete standard codes used in the design but also in terms of damage induced by aging and deterioration.

KEYWORDS

corrosion, incremental static analysis, nonlinear FE analysis, RC core-wall irregular building, seismic fragility assessment, time-dependent fragility curves

1 | INTRODUCTION

Seismic risk assessment of existing reinforced concrete (RC) buildings has drawn the attention of the scientific community and public administrations, driven by the need to reduce the huge economic losses registered

Discussion on this paper must be submitted within two months of the print publication. The discussion will then be published in print, along with the authors' closure, if any, approximately nine months after the print publication.

during recent earthquakes, especially in the Mediterranean area.[1] On the one hand, these losses are strictly connected to the increasing complexity of urban systems and the high population density of city centers, with their obvious impact in terms of exposure.[2] On the other hand, the vulnerability of the existing building stock is intrinsically high, since the large majority of RC buildings across Europe were realized without construction details able to cope with seismic actions, or following obsolete seismic design codes.[3] Furthermore, this vulnerability is intended to inevitably increase over time, due to material degradation associated with aging and lacking or ineffective maintenance.[4,5]

One of the most widely used tools for the assessment of damage in earthquake scenarios is represented by fragility curves, which express the conditional probability that a certain limit state is exceeded at a given value of ground-motion intensities, spanning over a wide range of relevant values.[6–8] According to the data reported in[9] for RC buildings, up-to-date fragility assessment studies have essentially concerned moment-resisting (MR) framed structures for a twofold reason. The first and most obvious reason is that MR frames are one of the most widespread structural typologies among existing RC buildings in Europe. The second aspect is related to the inherent simplicity of this structural system (with respect to others, like infilled frames or dual frame–wall systems), which makes numerical simulations easier to deal with and, to some extent, more reliable. However, in Italy, a significant number of existing RC buildings in large urban areas are characterized by the presence of a framed structure coupled with RC core-walls around the stairs and/or elevator. Many of these buildings date back to the period ranging from 1980 to 2000, and were then realized before the entry into force of modern seismic codes in the country; as a consequence, they were designed to sustain only gravity loads and wind action, disregarding the current seismic requirements. On the one hand, the presence of shear walls produces an increase in the sustainable base shear, while reducing at the same time forces and moments in frame elements. On the other hand, in most cases, the asymmetric position in the plan of core walls gives rise to a structural irregularity that may lead to torsional motions under seismic actions and dangerous stress concentration in some perimetral frame elements. This represents a further complication in the assessment criteria for the definition of damage states associated with fragility curves, making the extendibility to core-wall buildings of engineering demand parameters (EDP) commonly adopted for frames not so obvious.[10–13]

Another aspect of concern is that seismic risk assessment of the existing RC building stock is commonly performed with reference to initial values of material properties and strengths, so neglecting the effect of progressive deterioration due to time-dependent phenomena on the structural performance of the building. However, one of the primary sources of structural degradation is represented by reinforcement corrosion caused by exposure to environmental agents, namely carbonation and chloride attacks. As known, corrosion evolves over time, causing not only a reduction of rebar cross-section but also a decrease in the strength and deformation capacity of steel, and the deterioration of bond strength between bars and surrounding concrete. Corrosion is also responsible for the cracking and spalling of concrete cover, for the degradation of concrete compressive strength, and the reduction of confinement action on longitudinal rebars, so possibly determining the appearance of buckling effects. These phenomena are often amplified by the inadequate thickness of concrete cover and poor mechanical properties of materials, which are quite typical in RC buildings realized in the last century. It results in an increased vulnerability of the building stock under seismic events,[14–17] with a reduction in the load-carrying capacity of the structure and a shift toward more brittle failure mechanisms, especially for higher corrosion levels.[4,15]

This study aims at investigating the seismic performance of existing RC core-walls buildings with corroded steel rebars, exposed to different levels of corrosion. The problem is afforded through refined numerical analyses carried out with Abaqus, and focusing the attention on a testbed, representative of the investigated structural typology.[18] The seismic response of this testbed was already analyzed by the same authors in previous works,[11,12] with reference to the uncorroded situation. The proposed procedure and the choice of appropriate demand parameters for the definition of damage states in the case of RC core-wall buildings are further deepened in this study, where it is also validated through comparisons with other results from the literature referred to both RC framed structures and dual systems. Moreover, to assess the seismic performance of the considered building and its deterioration over time, pushover analyses are herein performed for different time periods and time-dependent fragility curves are then obtained through a procedure based on incremental static analysis,[19,20] as a function of the assumed corrosion rate.

The nonlinear behavior of corroded RC walls is taken into account through PARC_CL_2.1 crack model for RC elements subjected to cyclic loading. The PARC_CL_2.1 derives from PARC model, previously developed at the University of Parma for RC structures under static loads and based on a total fixed crack approach.[21] The PARC_CL_2.1 allows simulation of the reduction of reinforcement cross-section induced by corrosion, and it also

implements appropriate constitutive laws for steel, able to represent the buckling of uncorroded and corroded bars.[22,23] The effect of corrosion on frame elements is instead not explicitly included in numerical simulations but is simply applied during postprocessing of the results of pushover analyses, for the derivation of damage states to be used in the construction of fragility curves. To this end, ultimate chord rotation in columns is properly modified through the application of a reduction factor calibrated on the basis of experimental results.[24]

Since a limited number of studies on fragility assessment of irregular RC core-walls buildings subjected to corrosion are so far available in the scientific literature, the results of this work can be useful in providing a better understanding of the seismic vulnerability for the investigated structural typology. Finally, the concept of time-dependent fragility curves able to consider aging and corrosion effects on existing structures could help not only in assessing their present situation, but also in predicting the evolution of the seismic risk over time. If this concept is becoming quite established in the case of RC bridges, as proven by the increasing number of papers published on this topic, the derivation of time-dependent fragility curves for aging RC buildings is far less common up to date, and it is almost exclusively related to the case of framed structures.[25]

2 | CASE STUDY BUILDING AND MODELING ASSUMPTION

A six-story RC framed building with an internal asymmetric core[11] is selected as a testbed in the performed numerical analyses (Figure 1). This case study is deeply discussed in some University books for civil engineers,[18,26] as it is representative of existing RC core-walls buildings in large urban areas of Northern Italy designed for gravity loads only. The structure consists of three longitudinal frames, with spans of variable length (between 2.8 and 5.2 m), and two transverse frames, with two bays having the same span (5.7 m), placed along the building perimeter (Figure 1). Since the building is designed for gravity loads, primary frames, which are equipped with beams connecting the columns, are only oriented along the x direction, perpendicular to the joists used to realize the diaphragm (according to Figure 1). Therefore, columns result not connected with beams along the y direction, apart from the perimetral beams. Typical columns have cross-sections of 300×300 mm^2 or 300×400 mm^2, except in the inner longitudinal frame, where the cross-section of internal columns is variable along the height (from 500×400 mm^2 at the lower level to 300×400 mm^2 at the top one). The main geometric features and the reinforcement layout assumed for RC columns at different levels are summarized in Table 1, with reference to the nomenclature reported in Figure 1.

Beams have the same thickness as the floor slabs (240 mm), with a basis equal to 120 mm for the internal frame, and equal to 30 and 50 mm for the perimetral ones (in the transverse and longitudinal direction, respectively). Core walls have a thickness of 20 mm and are reinforced with ϕ12/300 mm longitudinal rebars and ϕ8/300 mm transverse rebars. The walls are designed to sustain wind load by considering a conventional

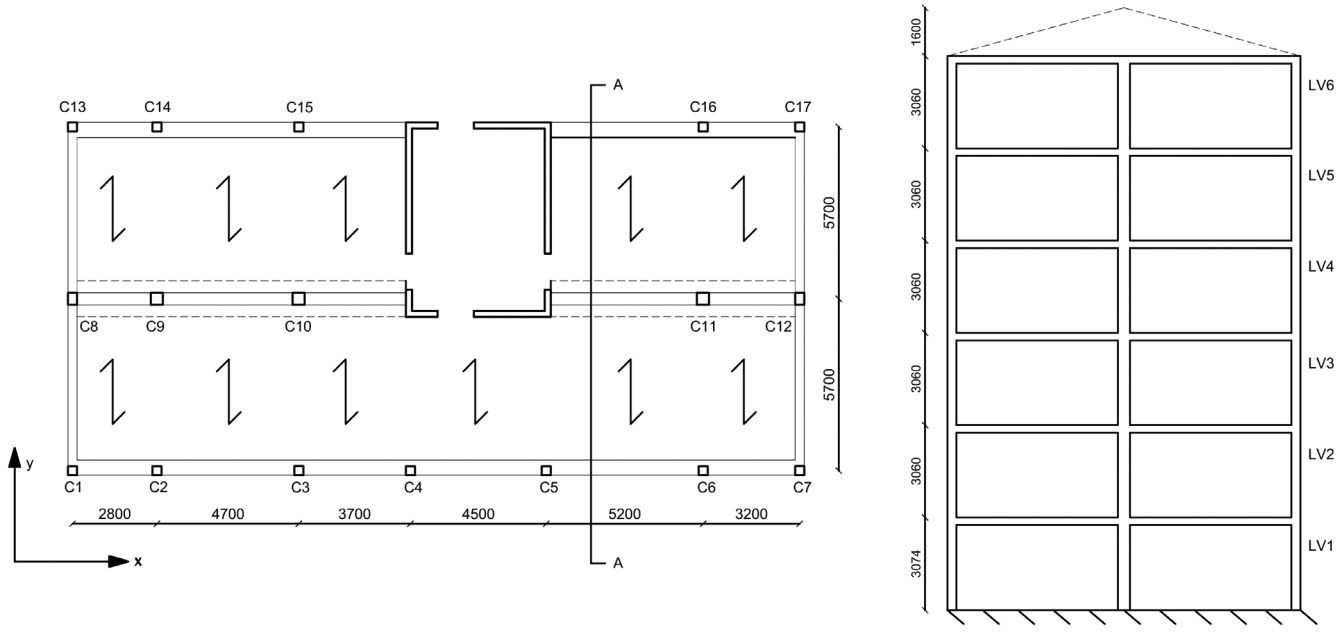

FIGURE 1 Geometry of the examined building: Typical floorplan and section AA (dimensions in mm)

TABLE 1 Geometric dimensions and reinforcement layout of RC columns at different levels

	Column ID									
	C1–C3–C4–C7–C13–C15–C17		C9–C10–C11		C8–C12		C5		C2–C6–C14–C16	
Level	$b \times h$ (mm^2)	$A_{s,tot}$ (mm^2)	$b \times h$ (mm^2)	$A_{s,tot}$ (mm^2)	$b \times h$ (mm^2)	$A_{s,tot}$ (mm^2)	$b \times h$ (mm^2)	$A_{s,tot}$ (mm^2)	$b \times h$ (mm^2)	$A_{s,tot}$ (mm^2)
LV6	300 × 300	4ϕ12	300 × 400	4ϕ12	300 × 400	4ϕ12	300 × 300	4ϕ12	300 × 300	6ϕ12
LV5	300 × 300	4ϕ12	300 × 400	4ϕ12	300 × 400	4ϕ12	300 × 300	4ϕ12	300 × 300	6ϕ12
LV4	300 × 300	4ϕ12	300 × 400	4ϕ12	300 × 400	4ϕ12	300 × 300	4ϕ12	300 × 300	6ϕ12
LV3	300 × 300	4ϕ12	400 × 400	4ϕ14	300 × 400	4ϕ12	300 × 300	4ϕ12	300 × 300	6ϕ12
LV2	300 × 300	4ϕ12	400 × 400	6ϕ14	300 × 400	4ϕ12	300 × 300	4ϕ12	300 × 300	6ϕ12
LV1	300 × 300	4ϕ12	500 × 400	8ϕ14	300 × 400	4ϕ12	300 × 300	6ϕ12	300 × 300	6ϕ12

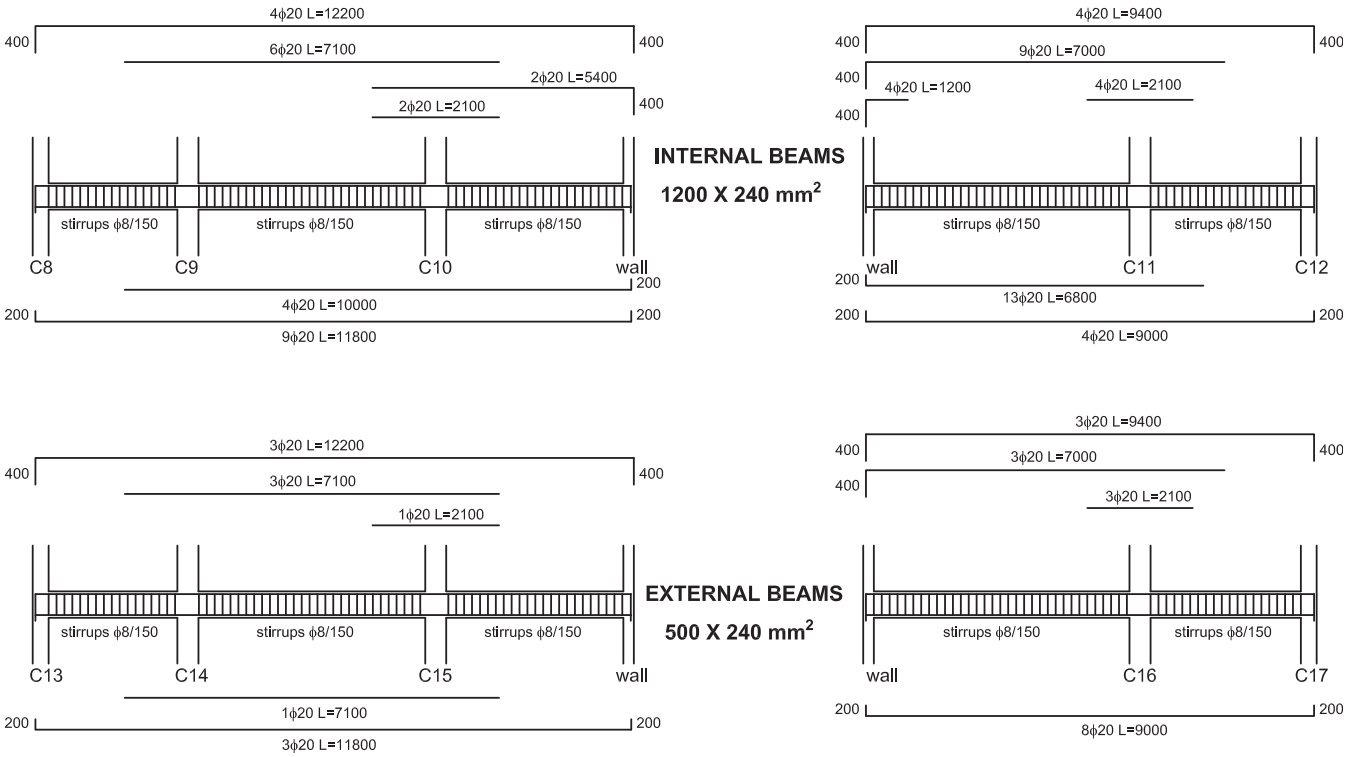

FIGURE 2 Typical reinforcement layout assumed for the main beams belonging to internal and external longitudinal frames (dimensions in mm, see Figure 1 for columns' nomenclature)

horizontal action equal to 0.5% of the weights (according to[18]). The typical reinforcement layout of the main beams belonging to the internal and external longitudinal frames, and of the core walls are shown in Figures 2 and 3, respectively. The characteristic value of concrete cylindrical compressive strength is assumed equal to 25 MPa, while steel reinforcement has characteristic yielding stress of 450 MPa. Floor slabs behave as rigid diaphragms since they are formed by RC joists and hollow clay blocks, with a 40 mm RC topping.

In this study, the building is supposed to be placed near the cost, and so it is exposed to airborne salt but not in direct contact with seawater, which is compatible with a XS1 exposure class. Numerical analyses are firstly carried out with reference to the uncorroded situation ($t = 0$) and then repeated at two different ages of the building ($t = 50$ years and $t = 100$ years), with the aim to simulate the effect of different corrosion levels. Corrosion is applied only at the lower level of the building, hosting garages and basements, since typically this part is the

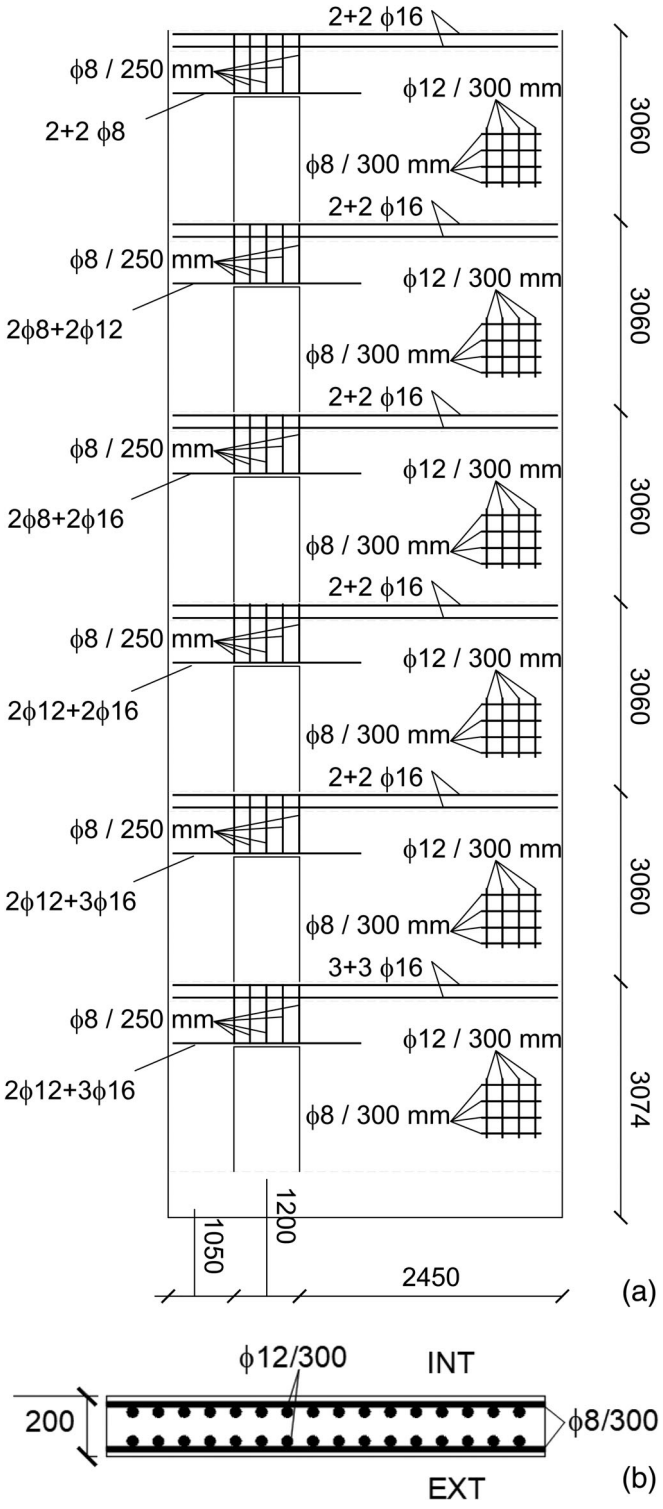

FIGURE 3 Typical reinforcement layout for core walls, (a) elevation view of one wall in the *x*-direction and (b) transverse cross-section (dimensions in mm)

more susceptible to deterioration. This is partly due to scarcer maintenance of basements with respect to main floors, but above all to the higher humidity level and to the more aggressive conditions that usually characterize the lower part of the building near foundations with respect to the rest of the structure. Two different scenarios are considered:

- in the first case, corrosion is only applied to RC walls, assuming that columns are properly coated (Figure 4a, corroded elements in dark red);
- in the second case, the attack of corrosion is applied to both walls and columns (Figure 4b, corroded elements in dark red).

In this way, it is possible to perform a first evaluation of the impact of corrosion on the global behavior of the testbed with respect to different possible configurations.

2.1 | Structural model

A general view of the adopted FE model is reported in Figure 4. The same modeling assumptions, which are discussed in the following, are applied both in the case of uncorroded elements and in the case of corrosion. RC columns and beams belonging to the frame are modeled with beam elements, specifically with three-node quadratic elements (B32) for columns and two-node linear elements (B31) for beams. Eight-node shell elements with reduced integration (S8R) and three Simpson integration points for each layer along the element thickness are used for the modeling of RC walls. To reduce computational efforts, one-layered shell elements are used to model the uncorroded parts of the walls, by smearing the reinforcement in the wall thickness and considering it applied in the mean plane of the wall. This assumption seems reasonable since in the examined case the walls mainly work in their own plane, while in the case of predominating out-of-plane behavior, it would be better to consider more layers in the modeling. In the case of corroded walls, two-layered shell elements are, however, introduced in the FE model. Indeed, the modeling of the corroded parts of the walls requires distinguishing between the reinforcement of the external corroded layer and the internal uncorroded layer (according to the assumed corrosion penetration depth at different times, discussed in Section 2.3), as depicted in the sketch reported in Figure 5. The effect of rigid floor slabs is implemented in the model through the kinematic coupling condition available in Abaqus software, which consists in constraining the motion of all nodes belonging to the slab to the rigid motion of an assigned master node. Both columns and walls are connected through fully supported rigid connections (with all degrees of freedom restrained) to the ground. In this study, the presence of infills realizing vertical closures of the framed structure is neglected for sake of simplicity.

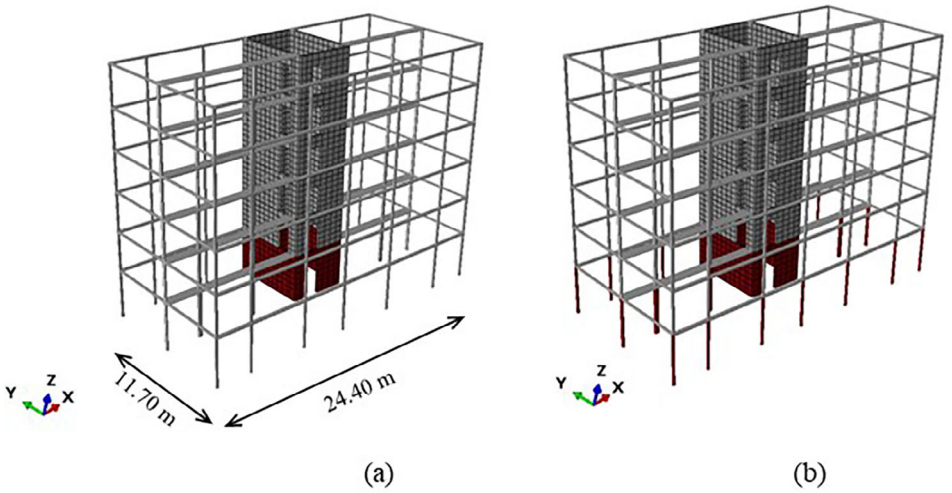

FIGURE 4 Finite-element model of the case study implemented in Abaqus in case of: (a) coated columns (b) uncoated columns (corroded elements in dark-red)

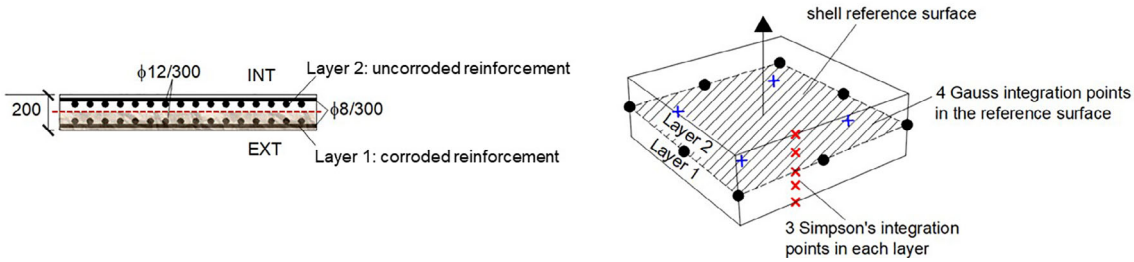

FIGURE 5 Layered shell elements adopted in case of corroded external reinforcement

2.2 | Modeling of materials' behavior in the initial configuration of the building (uncorroded)

The non-linear behavior of RC walls is evaluated by adopting the PARC_CL_2.1 crack model for RC elements subjected to cyclic loading.[22] The model, which is based on a smeared fixed crack approach, is implemented into Abaqus as User MATerial (UMAT) subroutine. It has been developed for multi-layered shell or membrane elements, by assuming the reinforcement as smeared within the concrete element through the geometric steel ratio. The PARC_CL_2.1 allows us to realistically represent plastic and irreversible strains in the unloading–reloading phase, thanks to its tangent approach and the constitutive laws implemented for the simulation of all nonlinear contributions (concrete in tension and compression, aggregate interlock, and tension stiffening) in case of cyclic actions. With respect to the original version of the model for cyclic loads (PARC_CL_2.0,[27]), the PARC_CL_2.1 implements different stress–strain relationships for steel, from the widely used model of Menegotto-Pinto,[28] to the models of Monti-Nuti[29] or Kashani and others,[30] which are able to detect buckling of reinforcement. In its last release, time-dependent effects and corrosion of reinforcement are also included[23] (Section 2.3).

Nonlinear behavior of frame elements is instead modeled by assigning a nonlinear moment–curvature law at the integration points of beam elements. The nonlinear moment–curvature law is inputted on the basis of the results of a sectional analysis carried out by adopting Saenz law with ultimate strain equal to 3.5×10^{-3} for concrete and an elastic-perfectly plastic law for steel. For columns, the resisting cross-sectional moment M_{Rd} is determined as a function of the acting axial load N, obtained from tributary areas. For sake of simplicity, M–N interaction is instead neglected in this study.

2.3 | Modeling of corrosion effects in RC walls

In the case of RC walls, the effect of material deterioration due to environmental factors is once again modeled by PARC_CL_2.1 crack model, where appropriate constitutive relations for concrete and steel damaged by corrosive phenomena[31] have been implemented. Since the testbed is assumed to be placed in the marine environment, chloride-induced corrosion is considered, by

assuming an environmental condition comparable to XS1 exposure class. Besides the initial uncorroded stage ($t = 0$ years), the seismic behavior of the structure is analyzed for the other two ages of the structure, respectively, equal to $t = 50$ years and $t = 100$ years, corresponding to the nominal life of ordinary residential buildings (that can be considered almost completely passed) and to its double.

The first step of the followed procedure consists of the evaluation of the reduction of reinforcement cross-section due to corrosion deterioration. This requires the preliminary determination of time intervals associated with corrosion initiation, t_i, and corrosion propagation, t_p, according to Tuutti's model.[32] By applying the second Fick's law and assuming that the chloride surface concentration C_{sa} and the chloride diffusion coefficient D_{cl} in concrete remain constant, chloride concentration $C(x,t)$ at a given depth x at the time t can be calculated through the following expression[33]:

$$C(x,t) = C_i + (C_{sa} - C_i)\left[1 - erf\left(\frac{x}{2\sqrt{D_{cl}\,t}}\right)\right], \quad (1)$$

where it is posed: $C_i = 0$ (initial chloride content), $C_{sa} = 0.45\%$,[33] and $D_{cl} = 0.61$ cm^2/year (as discussed in[31]), while erf is the error function. Figure 6 shows the evolution of chloride content over time for the considered exposure class. An initiation period of about 33 years can be obtained from calculations, corresponding to the time that the penetration depth of chloride ions—characterized by a critical chloride content C_{cr} equal to 0.25%—requires to reach the concrete cover value, equal to 35 mm. Afterward, a propagation period $t_p = t - t_i$ equal to 17 and 67 years is derived for the two considered assessment intervals of 50 and 100 years, respectively.

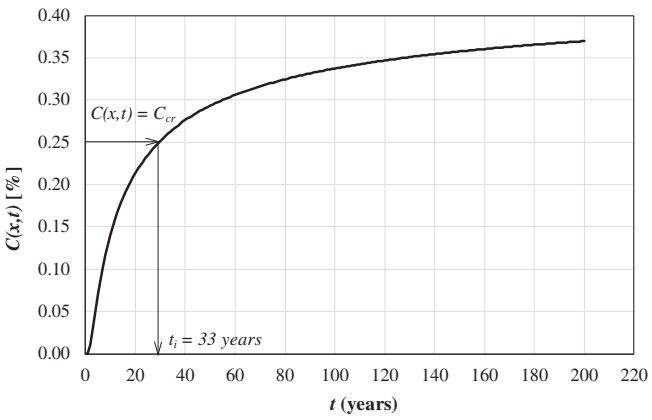

FIGURE 6 Evolution of chloride content over time for the considered exposure class XS1

As known, chlorides usually produce a localized attack on rebars, known as pitting. In order to determine the reduced bar cross-section due to pitting, the maximum penetration depth P_{pit} at time t_p (representing the loss in cross radius) should be first calculated, according to[34]:

$$P_{pit}(t_p) = 0.0116\ \alpha\ t_p\ I_{corr}, \quad (2)$$

where 0.0116 is a conversion factor of μA/cm^2 into mm/year, α is the pitting factor, and I_{corr} is the corrosion rate. As suggested in,[34] in this work, the following values are assumed: α = 10 and I_{corr} = 2.5 μA/cm^2, the latter lying in the range suggested by CONTECVET manual in case of exposure to airborne seawater.

Starting from this maximum penetration depth, the area loss due to pitting $A_p(t_p)$ is calculated by assuming a hemispherical pit-type morphology configuration through the expressions proposed by Val[35] (see also[31,36]), and then the maximum cross-sectional loss over time is determined as:

$$\mu_{max} = \frac{A_p(t_p)}{A_{s0}}\ 100 \quad (3)$$

where A_{s0} is the cross-section of the uncorroded rebar. The so obtained values are summarized in Table 2, with reference to the diameters of rebars forming the walls' reinforcement: ϕ12 mm and ϕ8 mm for the current reinforcing grid; ϕ12 and ϕ16 mm for the longitudinal bars of the lintel above the stairs' door, and ϕ16 mm for the ring beam reinforcement at floor level, according to the reinforcement layout reported in Figure 3.

Apart from rebar cross-section reduction, many experimental tests have highlighted the negative impact of corrosion on steel ductility. To take into account this aspect, the ultimate steel strain is properly reduced in numerical analyses through the expression proposed by Chen and others,[37] as better discussed in,[31] to which reference is made.

The propagation of corrosion is also associated with the formation of corrosion products (rust), which cause concrete cracking and spalling as the volume of rust increases. To consider this effect in numerical analyses, it is assumed

TABLE 2 Maximum cross-sectional loss over time for the rebars forming walls' reinforcement

Uncorroded diameter of walls' reinforcement (mm)	μ_{max} (%) $t = 50$ years	μ_{max} (%) $t = 100$ years
8	55.2	100
12	27.8	100
16	16.5	100

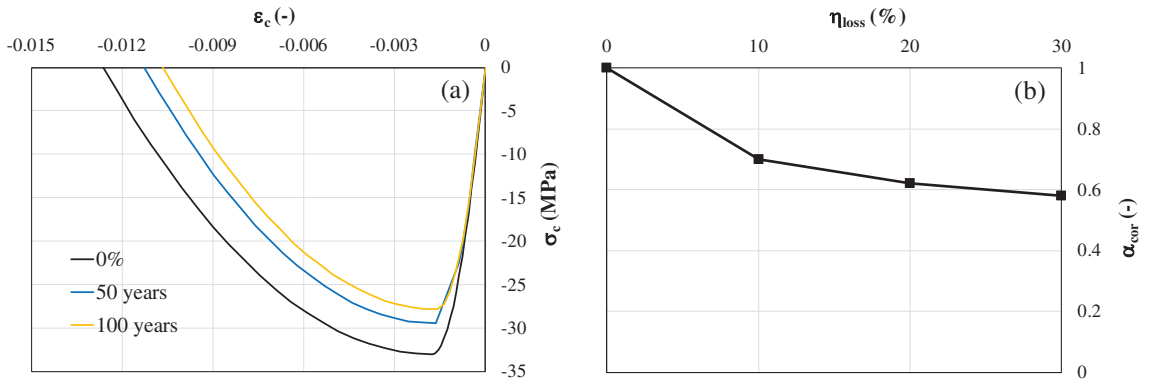

FIGURE 7 (a) Stress–strain relation for concrete in compression (mean values) and its variation over time; (b) reduction factor to be applied to ultimate chord rotation of columns, as function of the mass loss for a reinforcement diameter equal to 16 mm, according to[24]

that concrete cover spalling takes place when rebar mass loss η_{loss} reaches a threshold value, equal to 20%.[38] When this condition is satisfied, the thickness of shell elements used for the modeling of RC walls is properly reduced in the corroded layer. Mass loss is determined as[39]:

$$\eta_{loss} = \frac{1 - \frac{A_{corr}(t_p)}{A_{s0}}}{0.0161} \tag{4}$$

where $A_{corr}(t_p)$ is the corroded area of the rebar over time, namely the difference between the initial uncorroded area A_{s0} and the area loss due to pitting $A_p(t_p)$. The performed calculations highlight that even after 100 years the corrosion process only affects the external layer of the wall reinforcement, without reaching the internal one. Consequently, uncorroded properties are always assumed for the internal layer of the walls.

Finally, in those regions where concrete cover is spalled, concrete compressive strength and ultimate strain are properly reduced over time according to the formulation discussed in,[31] as depicted in Figure 7a.

2.4 | Modeling of corrosion effects in RC columns

The possible occurrence of anticipated brittle failure mechanisms in the elements of the framed structure is not investigated in this study. The effect of corrosion deterioration is herein taken into account in a simplified way, by only considering its negative impact on element ductility, in terms of the reduction of ultimate chord rotation of RC columns placed at the lower level of the testbed. As better discussed in,[40] the detrimental effects of mass loss reduction in terms of ductility are indeed much more pronounced near failure than in correspondence of yielding (as depicted in Figure 8a, adapted from[40]). The same study[40] reveals that corrosion has a negative impact also in terms of columns' bearing capacity, but this aspect is not taken into account in the performed study, since for sake of simplicity all the analyses are performed by inputting the moment–curvature relation for uncorroded columns, and by acting on ultimate chord rotation in the postprocessing of the results, as better described in the following. On this aspect, it should be, however, kept in mind that the resistant contribution provided by the frames against lateral loads is quite limited, as proved by the comparisons between the structural response of the building with nonlinear collaborating frames and that of the same building with pendulum frames reported in[11] (see also Figure 8b).

Ultimate chord rotation can be determined according to the formulation reported in Eurocode 8, Part 3,[41] for the uncorroded situation:

$$\theta_u = \frac{1}{\gamma_{el}} 0.016 (0.3^{\nu}) \left[\frac{\max(0.01;\omega')}{\max(0.01;\omega)} f_c \right]^{0.225} \left(\frac{L_v}{h} \right)^{0.35} 25^{\left(\alpha \rho_{sx} \frac{f_{yw}}{f_c}\right)} \left(1.25^{100\rho_d}\right) \tag{5}$$

where γ_{el} is equal to 1.5 for primary seismic elements and 1 for secondary seismic elements; h is the cross-section depth; and L_v is the moment/shear ratio at the end section; $\nu = N/(A_c f_c)$, where N is the axial load and A_c the concrete gross area; ω and ω' are the mechanical reinforcement ratios of longitudinal reinforcement in tension (including the web reinforcement) and compression; f_c and f_{yw} are concrete compressive strength (MPa) and stirrup yield strength (MPa), respectively; ρ_{sx} is the ratio of transverse steel parallel to the direction x of loading; ρ_d is

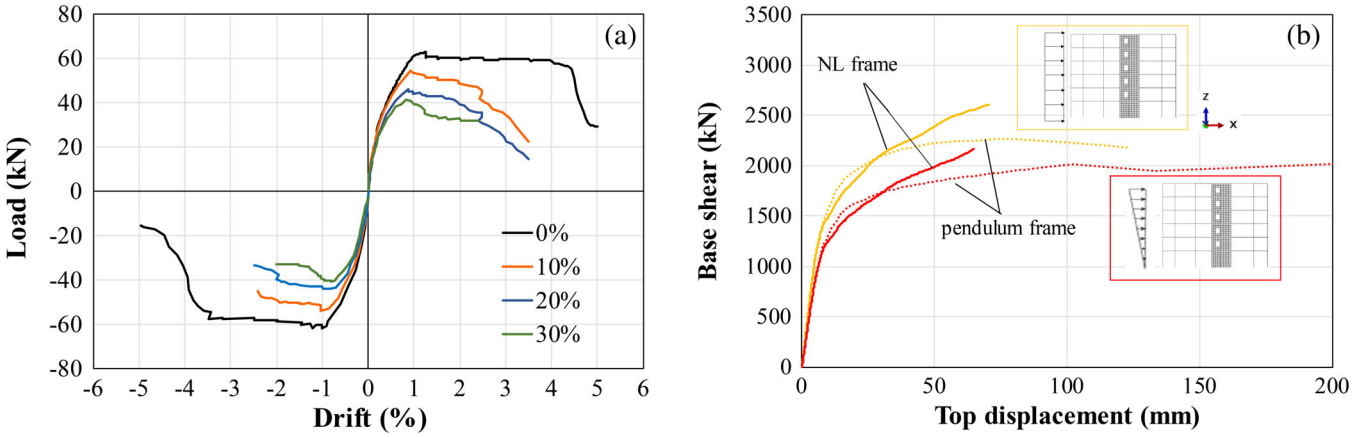

FIGURE 8 (a) Effect of corrosion of longitudinal reinforcement (ϕ16 rebars) on load–drift relationship (adapted from[40]); (b) evaluation of the resistant contribution offered by RC frames from PO curves

the steel ratio of diagonal reinforcement (if any), in each diagonal direction; and α is the confinement effectiveness factor. An extension of Equation (5) to the case of corroded elements was proposed in Vecchi and Belletti,[24] with the introduction of a reduction coefficient α_{cor}, which depends on rebar diameter and corrosion level (in terms of mass loss). This coefficient was calibrated on the basis of the results of numerical simulations, which were previously validated through comparisons with the experimental response of uncorroded and corroded RC columns, typical of existing pre-code Italian buildings, tested under cyclic loading.[42] For the sake of clarity, the dependency of the reduction coefficient α_{cor} from the mass loss is plotted in Figure 7b in case of ϕ16 mm rebars, which corresponds to the lower diameter considered in.[24] This relation has been herein applied to the columns of the considered building, despite the not perfect match of the diameters. From the performed calculations, in the investigated case study, the mass loss is equal to 10% for an assessment period t of 50 years, while $\eta_{loss} = 62\%$ for $t = 100$ years. Since the analytical relation between the reduction coefficient α_{cor} and the mass loss reported in Figure 7b was validated up to a value of 30%,[24] for $t = 100$ years an extrapolation is performed, although it may probably lead to conservative results. In this way, it is obtained $\alpha_{cor} \cong 0.7$ for $t = 50$ years, and $\alpha_{cor} \cong 0.3$ for $t = 100$ years. This reduction coefficient is applied to numerical results in the postprocessing phase, according to the following procedure. With reference to the uncorroded case, the first columns failing in bending among those of the lower level are initially detected, and their chord rotation is multiplied by the reduction coefficient α_{cor} previously determined. This updated chord rotation is then used for the definition of damage states associated with fragility curves, as better explained in Section 3.

3 | PUSHOVER ANALYSIS OF THE CASE STUDY BUILDING WITH AND WITHOUT CORROSION AND DEFINITION OF DAMAGE STATES

3.1 | Time-dependent capacity curves

PushOver (PO) analysis is widely used in seismic assessment of existing structures for the evaluation of the inelastic response under a lateral loading pattern. According to Eurocode 8, Part 3,[41] two distributions are considered in the performed analyses: (a) a modal pattern, with lateral forces proportional to the displacement shape of the first mode of vibration; and (b) a uniform pattern, with lateral forces proportional to the mass at each floor. Accidental eccentricity is applied by shifting the center of mass away from its original position, combining at the same time the two eccentricities in x and y directions, so to maximize the distance from the center of stiffness.[11] PO analyses are repeated along both x and y axes, in the positive and negative directions, for the three considered exposure times ($t = 0$, 50, 100 years). The main outcomes are reported in terms of capacity curves, which relate to the base shear and target displacement of the top level of the structure. In this case, the top displacement is set equal to the average of the displacements registered at two nodes, placed at the opposite corners of the roof floorplan.

The influence of different corrosion levels on the capacity curve is shown in Figure 9. Numerical results highlight that all curves have almost the same initial stiffness, but both lateral bearing capacity and global ductility reduce with increasing exposure times. It is worth noticing that these curves merely reflect the effect of corrosion in RC walls, since it has been already pointed out that the degradation of columns is only considered at a subsequent stage, during

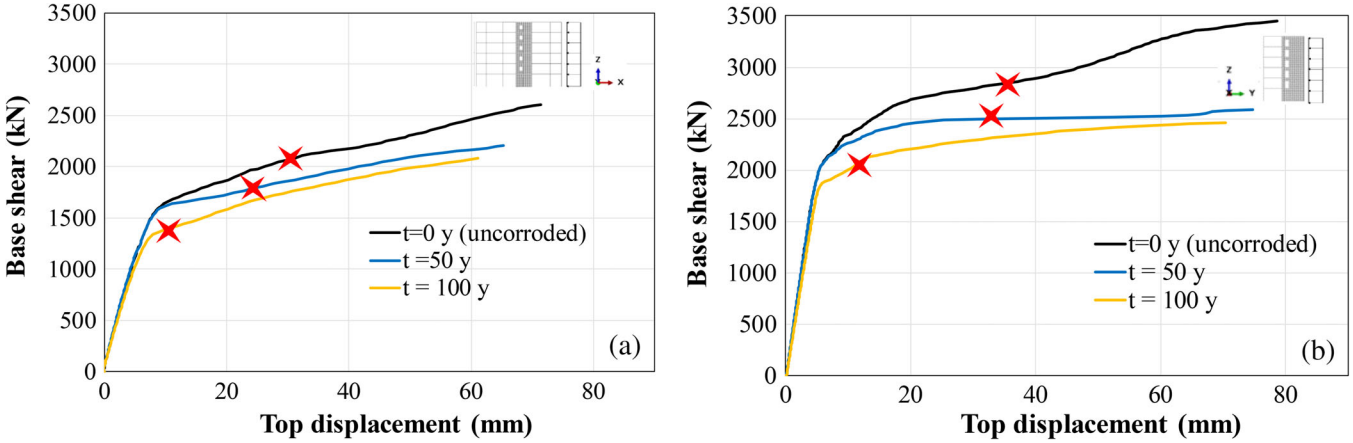

FIGURE 9 Base shear vs. top displacement curves for different exposure times for a uniform lateral load pattern acting along (a) –*x* and (b) –*y*

TABLE 3 Proposed damage thresholds

LS		1	2	3	4
EMS-98 definition					
		SD = null NSD = slight	SD = slight NSD = moderate	SD = moderate NSD = heavy	SD = heavy NSD = very heavy Destruction
Material-based EDPs (only for walls)		$\varepsilon_c = \varepsilon_{cracking}$ (cracking)	$\lvert\varepsilon_c\rvert = 3.5‰$ (concrete cover)	$\lvert\varepsilon_c\rvert = 3.5‰$ (confined concrete)	$\lvert\varepsilon_c\rvert = 3.5‰$ (*) (confined concrete)
			$\varepsilon_s = \varepsilon_y$	$\varepsilon_s = 1\%$	Buckling/failure longitudinal rebars
Material-based EDPs + CRC	Walls	$\varepsilon_c = \varepsilon_{cracking}$ (cracking)	$\lvert\varepsilon_c\rvert = 3.5‰$ (concrete cover)	$\lvert\varepsilon_c\rvert = 3.5‰$ (confined concrete)	$\lvert\varepsilon_c\rvert = 3.5‰$ (*) (confined concrete)
			$\varepsilon_s = \varepsilon_y$	$\varepsilon_s = 1\%$	Buckling/failure longitudinal rebars
	Columns	–	$\theta = \theta_y$	$\theta = ¾\ \theta_u$	$\theta = \theta_u$
Risk UE approach		$S_{d1} = 0.7\ d_y$	$S_{d2} = d_y$	$S_{d3} = d_y + 0.25\ (d_u – d_y)$	$S_{d4} = d_u$

Note: (*) pre-code, inadequately confined members.

the postprocessing of numerical results. However, to better highlight the reduction in terms of global ductility induced by corrosion in columns, in the same Figure 9, a red star is also reported on the curves when the first column at the lower level reaches the ultimate value of chord rotation.

3.2 | Choice of engineering demand parameters and damage state definition

The definition of damage thresholds for fragility assessment is strictly related to the identification of suitable structural response quantities, known as engineering demand parameters (EDPs). For RC framed buildings, the extent of damage is usually controlled by the Inter-Story drift Ratio (IDR), and quite consolidated drift threshold values associated with EMS-98 damage grades[43] can be found in the technical literature.[44] This type of approach is also followed in Hazus-MH 2.1 Technical Manual,[45] which refers to different building typologies, three different height categories (low, mid, and high rise), and four design levels. However, the use of IDR may be inappropriate in the case of RC core-walls, as discussed in.[11] On the other hand, FE analyses allow a detailed representation of damage

phenomena (cracking, crushing, yielding, and buckling) and their evolution as loading increases.[44] Therefore, damage thresholds can be more precisely identified with reference to material strain limits, similarly to the approach firstly introduced by Crowley and others.[46] Damage thresholds' identification based on material-based EDPs for irregular existing RC buildings with shear walls has been already proposed by some of the authors in,[11] according to Table 3 (see raw named "Material-based EDPs"). However, for building with RC walls and collaborating moment-resisting (MR) frames, it may be necessary to evaluate also the damage of frame elements. In case of ductile failures (as those expected for the testbed in its original uncorroded condition), one of the possible damage indicators is represented by chord rotation. According to Eurocode 8, Part 3,[41] in case of moderate damage (LS2), the rotation capacity is limited by the chord rotation corresponding to yielding, which can be calculated as:

$$\theta_y = \Phi_y \frac{L_v}{3} + 0.0013\left(1 + 1.5\frac{h}{L_v}\right) + 0.13\,\Phi_y \frac{d_{bL} f_y}{\sqrt{f_c}} \quad (6)$$

where Φ_y is the yield curvature of the end section; f_c and f_y are concrete strength and steel yield stress, respectively; and d_{bL} is the (mean) diameter of the tension reinforcement. For higher damage states, the chord rotation capacity is instead limited to ¾ of the ultimate rotation capacity (LS3) or to the ultimate rotation capacity (LS4), which can be calculated through Equation (5).

This further check on the chord rotation of the elements belonging to the frame is added to the control on material strains' limits in the walls, and the corresponding damage state is assumed to be reached when either one of these conditions (damage threshold in walls or columns) is achieved, according to Table 3, raw "Material-based EDPs + Chord Rotation Control (CRC)."

Another possible analytical approach for defining damage thresholds is the one developed within the Risk UE project,[47,48] which relates the first four damage grades of EMS-98 macro-seismic scale (the fifth one is considered coincident with the fourth one, as also assumed in the other approaches previously discussed) to the spectral displacements corresponding to two control points in the capacity curve, at yielding and at the ultimate condition, respectively (d_y and d_u). The spectral displacements corresponding to each damage threshold are summarized in Table 3, raw "Risk UE approach."

Based on the results obtained for the testbed, fragility curves derived by applying the Risk UE approach are comparable to those obtainable when referring to material-based EDPs, as will be better discussed in Section 4.

4 | VALIDATION OF THE PROCEDURE FOR THE UNCORRODED CASE AND DERIVATION OF TIME-DEPENDENT FRAGILITY CURVES

4.1 | Methodology applied for fragility assessment

A numerical procedure based on incremental static analysis (ISA) and discussed in[19] is used for deriving fragility curves (FCs). This approach is based on a generalization of the incremental N2 method[49,50] with the use of natural spectra, directly derived from recorded accelerograms that are usually adopted to perform time history analyses for incremental dynamic analysis (IDA). This allows reproduction of the record-to-record variability that distinguishes time history analyses, by reducing at the same time computational efforts and time. To perform ISA, eight PO curves are required (in $\pm x$, and $\pm y$ directions, for the two considered lateral force distributions), together with the indication of the four considered damage thresholds. As seismic input, response spectra corresponding to 125 spectrum-compatible accelerograms, referred to rigid soil condition and elaborated within DPC-ReLUIS research activities (WP4 MARS,[51]), are used in this work. According to the capacity spectrum method,[52] the capacity of the structure, in terms of PO curves, is compared with the demands of earthquake ground motion, in terms of response spectra. The performance point is first determined for each explored value of the PGA, starting from all the input spectra and capacity curves, and the worst situation is then considered. Finally, the cumulative probability of exceeding a given damage state is calculated and used for the construction of FCs. The possible application of N2 method with natural spectra implemented within ISA is illustrated in Figure 10, for two possible occurring situations, corresponding to the case of T* larger or shorter than T_C (being T* the period of vibration of the SDOF equivalent to the MDOF structure). Based on the results discussed in,[19] it can be demonstrated that ISA can be proficiently used for the construction of FCs. The obtained results are indeed slightly conservative with respect to those derived from IDA, but reasonably controlled differences between the two approaches, especially if on the safe side, can be

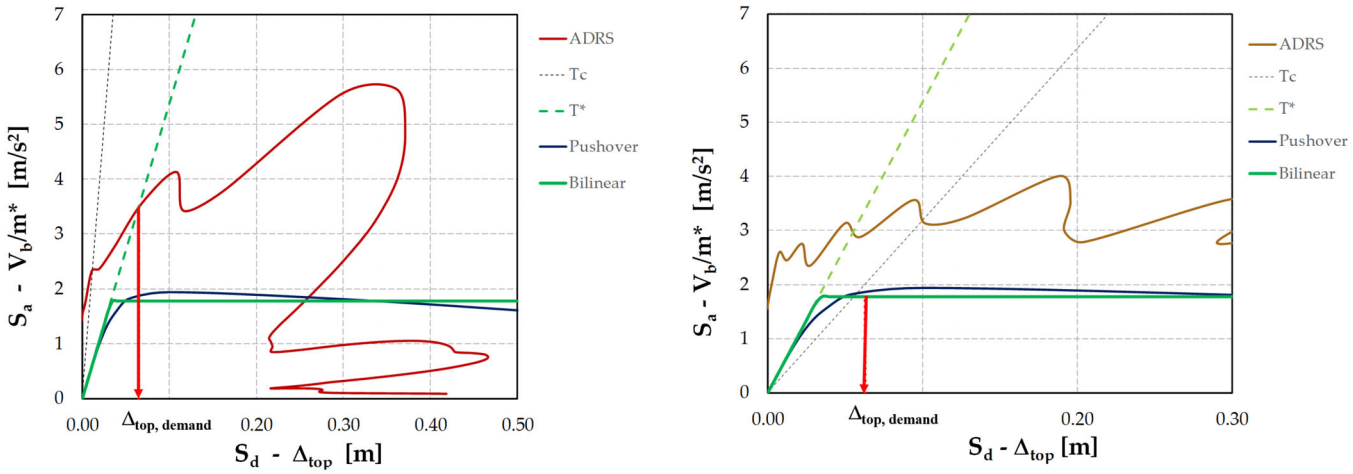

FIGURE 10 Schematic approach of the IN2 method applied within ISA

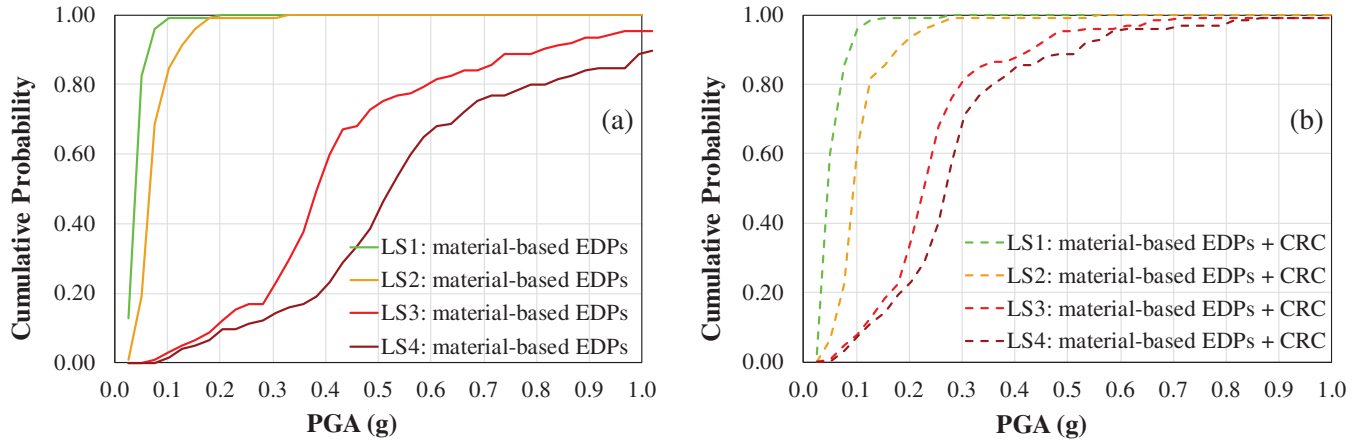

FIGURE 11 Fragility curves for the analyzed testbed in the uncorroded condition, obtained by defining damage thresholds for RC walls as function of material-based EDPs, (a) without and (b) with supplementary controls on chord rotation for columns (CRC)

considered acceptable in light of the high reduction of the computational burden.

4.2 | FCs for the reference uncorroded case: Validation of the proposed procedure and influence of EDPs choice

Figure 11 shows fragility curves obtained for the analyzed testbed in the original uncorroded situation, as obtained through the application of the ISA methodology, previously described.

In more detail, the curves plotted in Figure 11a are obtained by considering material-based EDPs for RC walls, without performing any control on the chord rotation for the columns of the lower level. The curves depicted in Figure 11b are instead obtained with reference to the damage thresholds defined in Table 3 for both walls and columns (material-based EDPs+ chord rotation control, CRC). The control on chord rotation of columns mainly affects LS3 and LS4 damage states, with a corresponding increased fragility of the structural system.

To validate the proposed procedure, the obtained results are compared with other fragility data available in the literature, which are relative to uncorroded structures (taken from[53]). Given the difficulty in finding other studies on irregular and complex RC dual systems designed for gravity loads only, the main criteria adopted in the selection of the data for the comparisons are related to the number of stories (mid-rise buildings) and the level of seismic design (pre-code or low code, i.e., with a low level of seismic design, roughly corresponding to pre-1980 codes in Europe). Figure 12a reports the comparison

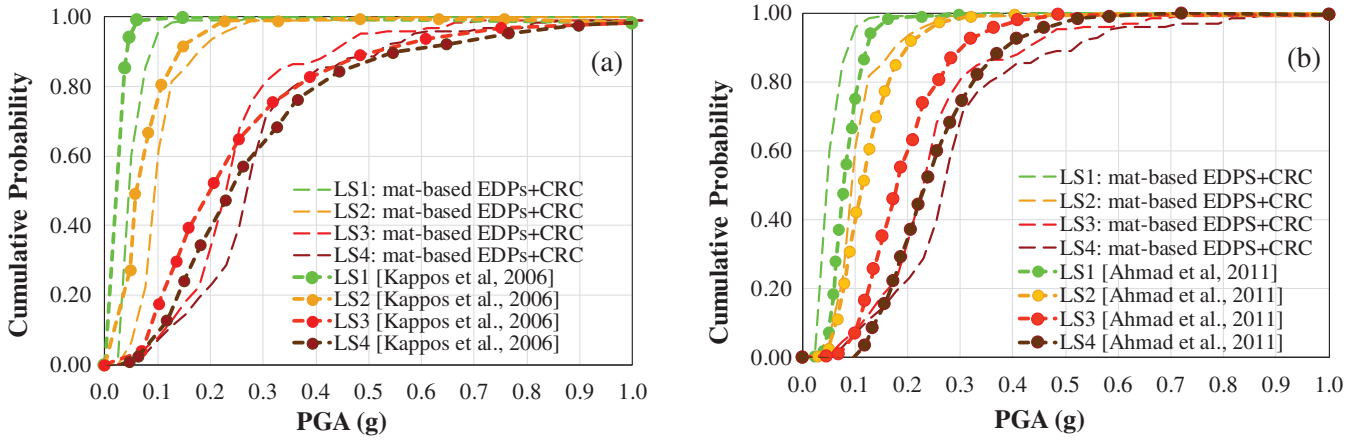

FIGURE 12 Comparisons among FCs for the testbed (according to damage threshold definition of Table 3) and the results discussed in: (a) Kappos et al.[54] for regularly infilled low-code mid-rise frames; and (b) Ahmad et al.[55] for irregular mid-rise RC framed buildings with non-ductile behavior

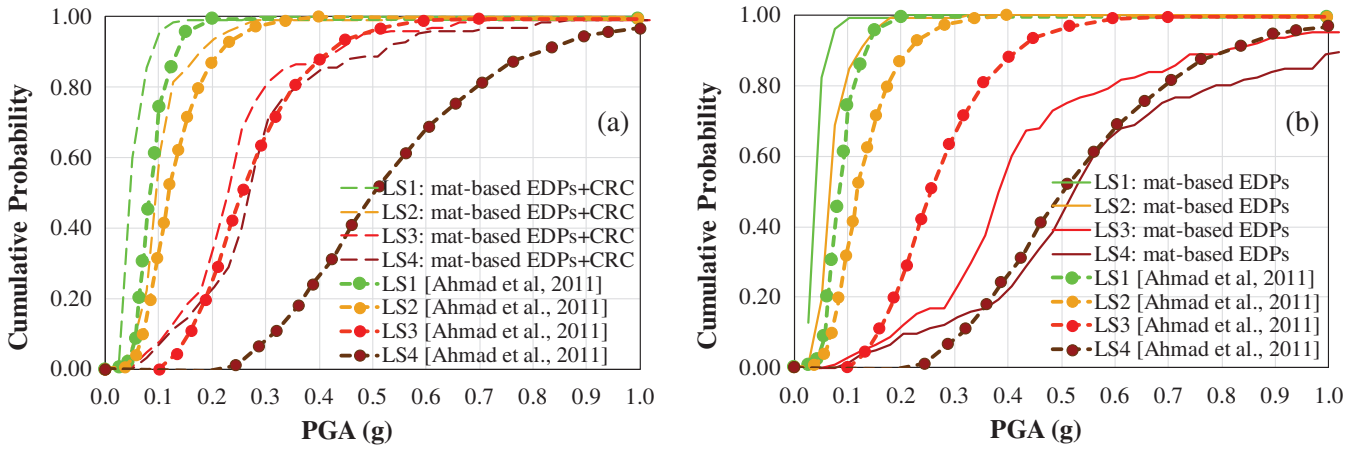

FIGURE 13 Comparisons between the results discussed in[55] with reference to irregular mid-rise RC framed buildings with ductile behavior, and numerical FCs for the testbed, by considering: (a) material-based EDPs for the walls and additional checks on chord rotation for columns, (b) only material-based EDPs for the walls

between FCs obtained for the testbed according to damage thresholds' definition reported in Table 3 and the results discussed in Kappos and others[54] for RC mid-rise low-code frames (with 4–7 stories), with regularly distributed infills. The latter curves were obtained through a hybrid approach, which combined the results of static and dynamic analyses. In Figure 12b, the same numerical FCs are compared with those obtained by Ahamad and others[55] for irregular RC framed buildings, with five stories (mid-rise) and characterized by non-ductile behavior. The curves reported in[55] were derived through an analytical approach, on the basis of nonlinear static analyses. Although the investigated structural typology in[54,55] is not the same as that of the present study, comparable results are obtained, also for higher damage levels, where failure is governed by the achievement of chord rotation's limits in columns. This could be partly explained by considering the strong influence exerted by building height and seismic design level on the structural vulnerability.

However, when looking at the results obtained by Ahamad and others[55] for irregular RC framed buildings, with five stories (mid-rise), and ductile behavior, a great scatter among the curves can be noticed, especially for LS4 damage state (Figure 13a). A more similar response can be instead obtained by removing the check on columns' chord rotation and defining damage thresholds with reference only to material strains' limits in the stair walls (Figure 13b).

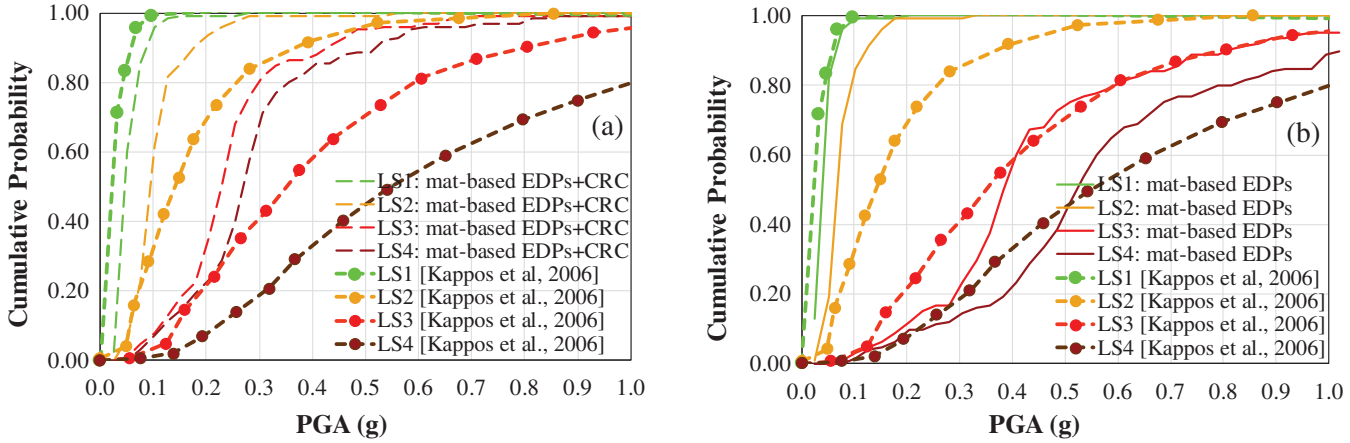

FIGURE 14 Comparisons between the results discussed in[54] for regularly infilled mid-rise RC dual systems, and numerical FCs for the testbed, by considering: (a) material-based EDPs for the walls and additional checks on chord rotation for columns, (b) only material-based EDPs for the walls

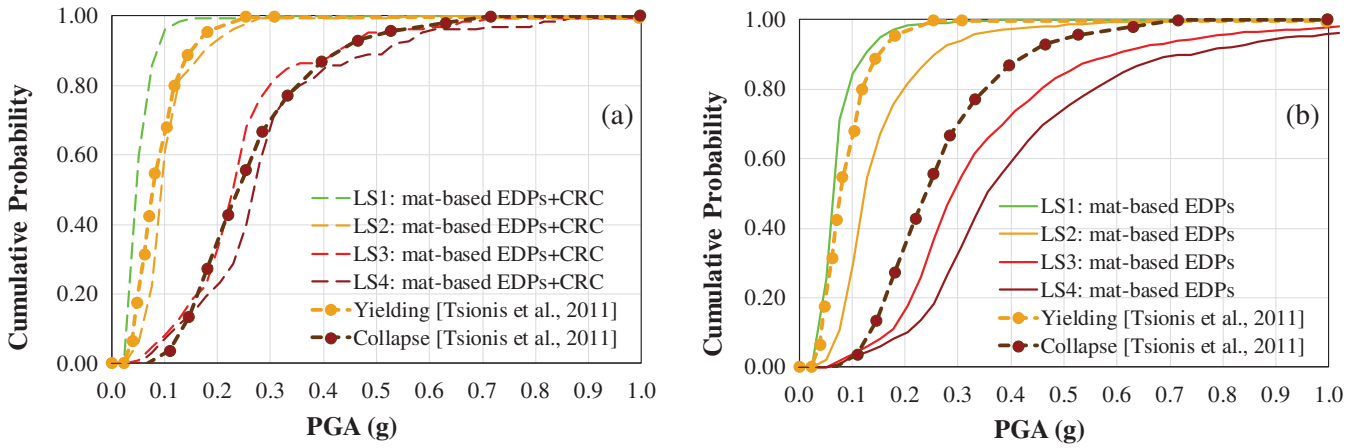

FIGURE 15 Comparisons between the results discussed in[56] for RC dual systems, high rise, designed with low code, and numerical FCs for the testbed, by considering: (a) material-based EDPs for the walls and additional checks on chord rotation for columns, (b) only material-based EDPs for the walls

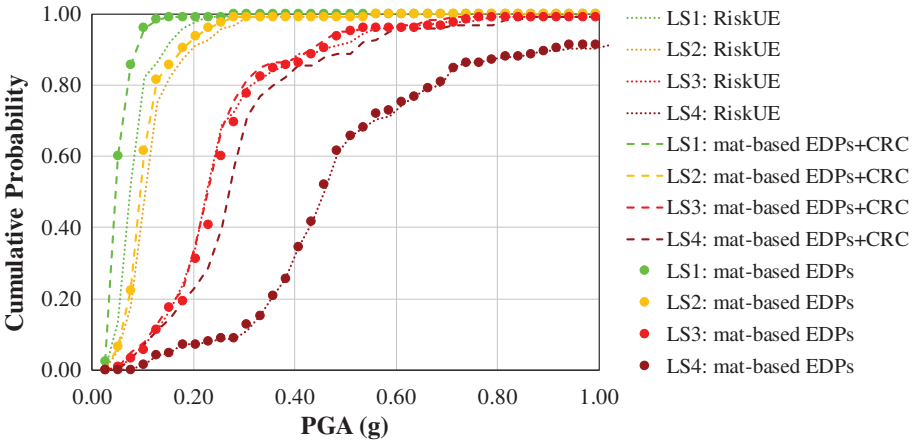

FIGURE 16 FCs for the testbed: Influence of the definition of damage thresholds

A comparison among numerical FCs obtained for the testbed and the curves obtained by Kappos and others[54] for regular infilled dual systems, with 4–7 stories (mid-rise) and low-code design, is reported in Figure 14. Also in this case, it can be noticed that a better agreement can be achieved by simply relating the damage thresholds' definition to the achievement of limit strain values in the walls' materials (concrete and steel, Figure 14b). On the contrary, additional checks on the rotational capacity of columns seem to lead to excessively conservative results (Figure 14a).

In Figure 15, the obtained FCs are compared to those derived by Tsionis and others[56] by means of nonlinear dynamic analyses for high-rise dual systems, designed with low code. In this last case, the greater agreement is obtained when considering damage to both walls and columns (Figure 15a), but the steeper trend of the curves reported in[56] may be also related to the difference in buildings' height (high-rise—8 or more floors vs. mid-rise—6 floors).

Finally, to better investigate the influence exerted by the choice of EDPs and damage thresholds on the final results for the investigated structural typology, a new set of FCs is derived for the testbed by applying also the Risk UE approach,[47,48] as discussed in Section 3.2. The results are depicted in Figure 16. It can be seen that the curves obtained through the application of the Risk UE approach and material-based EDPs for walls are almost superimposed, also for higher damage levels. For this reason, the Risk UE approach is chosen her for the evaluation of time-dependent FCs discussed in Section 4.3, since it requires easier postprocessing of analyses' results. However, it is important to remark that other studies on different RC core-walls buildings should be performed to

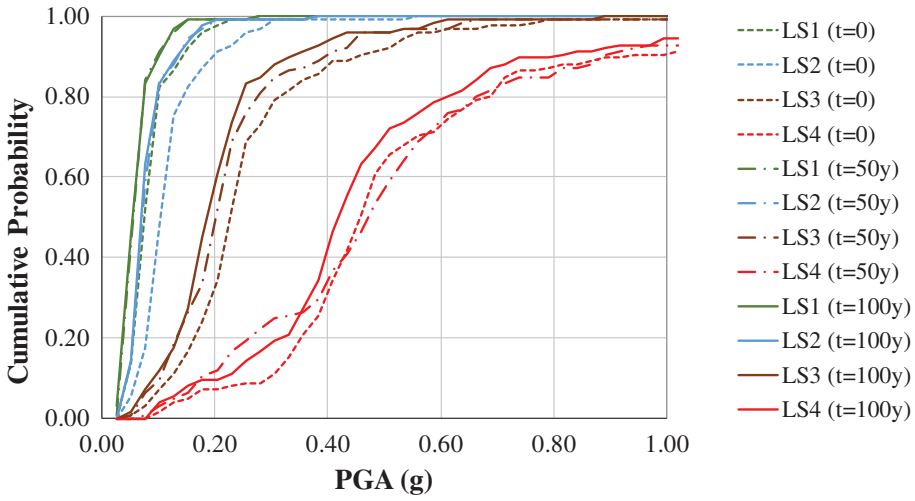

FIGURE 17 Time-dependent FCs for the case of corrosion applied only to the walls of the lower level.

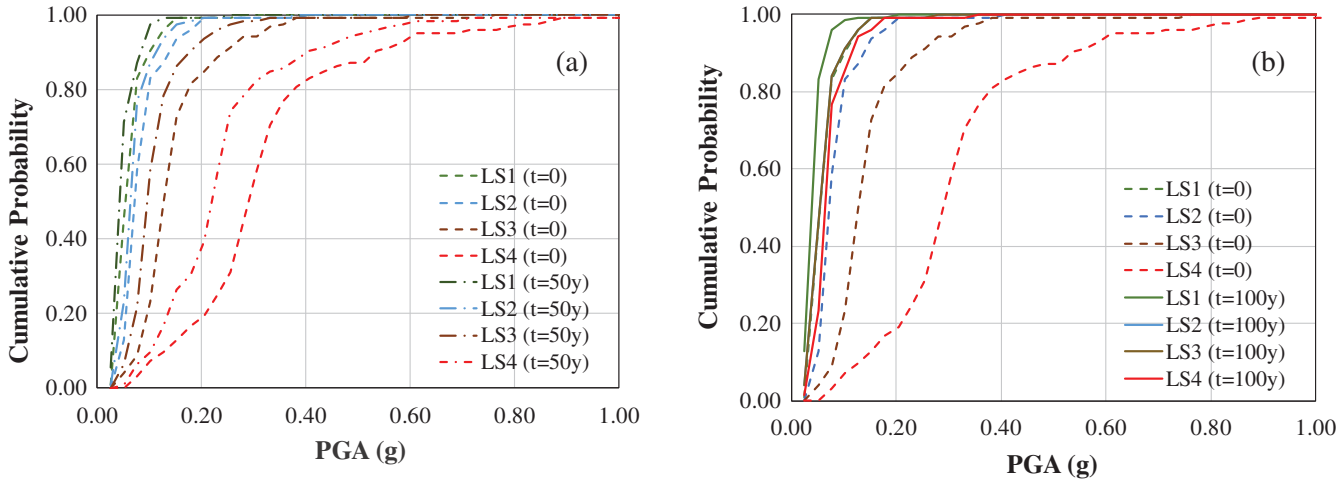

FIGURE 18 Time-dependent FCs for the case of corrosion applied to walls and columns of the lower level, comparison between the uncorroded reference case ($t = 0$) and the results obtained after (a) $t = 50$ years and (b) $t = 100$ years

reach a consensus on the relevant EDPs to be considered for RC wall buildings. If the control of columns' rotational capacity clearly leads to more conservative results, it is undoubtable that the collapse of one or more columns in dual systems will have a not negligible impact on the global behavior of the building, also in terms of intervention costs.

4.3 | Effect of corrosion on fragility curves

The effect of corrosion on the global structural response is highlighted through time-dependent fragility curves derived according to the Risk UE approach and plotted in Figure 17 (for the case with coated columns) and in Figure 18 (for the case with uncoated columns). As can be seen from Figure 17, the degradation due to the corrosion of wall reinforcement determines a progressive—but quite limited—increase in the collapse risk. A more significant impact of corrosion on the fragility curves of the building can be noted instead when also columns are subjected to corrosion, Figure 18. Based on the observations reported in the previous section, this effect is much more pronounced when referring to higher damage states, which are governed by the failure of columns. With reference to Figure 18, it can be also noted that the "buffer-zone" between LS3 (extensive damage) and LS4 (complete damage) significantly reduces for higher exposure levels, and consequently, the collapse risk increases significantly over time. For this reason, the curves are split into two separate graphs (respectively, comparing the results for $t = 50$ years and $t = 100$ years, with the reference uncorroded case) to improve their readability. On this point, it should be, however, remarked that the significant increase in failure probability obtained for $t = 100$ years (Figure 18b) directly derives from the reduction coefficient applied to the ultimate chord rotation of columns, since it has been obtained through extrapolation from the curve reported in Figure 7b, as already pointed out in Section 2.4. For $t = 50$ years, the mass loss is instead equal to about 10% and then the evaluation of the reduction factor is affected by fewer uncertainties.

Moreover, it is important to highlight that the reduction of the "buffer-zone" between extensive and complete damage (LS3 and LS4) is also related to the damage state definition according to the Risk UE approach. Indeed, since the ultimate displacement d_u on the PO is properly reduced based on the corrosion level achieved in the reinforcement (due to the reduction in chord rotation capacity of columns), this has a direct impact also on the definition of LS3 damage state, which corresponds to $S_{d\,LS3} = d_y + 0.25\,(d_u - d_y)$, where d_u reduces while d_y is kept unchanged.

5 | CONCLUSIONS

In this study, vulnerability assessment of existing irregular RC core-wall buildings is presented through a refined numerical approach, able to deal with the effects of material degradation and their impact on structural fragility. Based on the obtained results, the following aspects can be evidenced:

- for irregular RC core-wall buildings, the definition of suitable EDPs and damage thresholds required for the construction of fragility curves is still an open topic, although material-based EDPs referred to the control of strain limits in the materials of RC walls (concrete and steel) seem a promising solution;
- specifically, for the analyzed case study, this leads to results that are in very good agreement with those obtained by following the Risk UE approach, which is, however, easier to deal with, as it requires less effort during the postprocessing of the results; further investigations are needed by extending the comparisons to other testbeds;
- additional checks aiming at detecting possible damages and failures in columns, for example, through the achievement of chord rotation limits according to relevant Standard Codes, have a non-negligible influence on more severe damage states (especially LS4), leading to a more vulnerable response; however, the discussion is still open also on this topic, since the failure of frame elements in dual systems cannot be completely ignored, especially when estimating intervention and repairing costs;
- corrosion effects should be considered when deriving fragility curves for existing RC buildings, as their seismic capacity can be significantly overestimated especially in the case of more ancient structures, which have experienced a longer exposure to corrosion agents: the effect of corrosion seems to be much more pronounced in case of uncoated columns, but further investigations are needed for higher exposure times, also based on new experimental evidence.

Since the possible occurrence of brittle failure mechanisms in RC columns and nodes (that are outside of the scope of the study) can lead to even more severe results, this work should be intended as a preliminary study on the development of time-dependent fragility curves for RC core-wall buildings. Besides the specific results presented in this study, as the authors' aims, it should be considered as a comprehensive methodology to introduce material degradation effects (especially those due by chloride-induced corrosion of steel reinforcement) in seismic fragility analyses, which, in principle, can be adopted also for other types of RC structures.

ACKNOWLEDGMENT

This work was performed within DPC-ReLUIS2019-2021 project, task WP4—"MARS."

CONFLICT OF INTEREST

The authors declare no potential conflict of interest.

DATA AVAILABILITY STATEMENT

The data that support the findings of this study are available from the corresponding author upon reasonable request.

ORCID

Elena Michelini https://orcid.org/0000-0002-2262-0740
Beatrice Belletti https://orcid.org/0000-0002-4382-9930
Lorenzo Franceschini https://orcid.org/0000-0003-4826-4163
Enzo Martinelli https://orcid.org/0000-0003-3572-7528

REFERENCES

1. Tsionis G, Sousa ML, Palermo V, Maio R. Framework for resilience analysis of EU buildings. Luxembourg: Publications Office of the European Union; 2018. https://doi.org/10.2760/923762
2. Mouroux P, Le Brun B. RISK-UE project: an advanced approach to earthquake risk scenarios with application to different European towns. Assessing and managing earthquake risk. The Netherlands: Springer; 2008. p. 479–508.
3. Palermo V, Tsionis G, Sousa ML. Building stock inventory to assess seismic vulnerability across Europe. Proceedings of the 16th European conference on earthquake engineering. Luxembourg: Publications Office of the European Union; 2018. p. 18–21.
4. Karapetrou ST, Fotopoulou SD, Pitilakis KD. Seismic vulnerability of RC buildings under the effect of aging. Procedia Environ Sci. 2017;38:461–8.
5. Couto R, Sousa I, Bento R, Castro JM. Seismic vulnerability assessment of RC structures: research and practice at building level. Seismic vulnerability assessment of civil engineering structures at multiple scales. London: Elsevier; 2022. p. 31–84.
6. Fardis MN, Papailia A, Tsionis G. Seismic fragility of RC framed and wall-frame buildings designed to the EN-Eurocodes. Bull Earthq Eng. 2012;10(6):1767–93.
7. Papailia A, Tsionis G, Fardis MN. Seismic fragility of RC buildings designed to Eurocodes 2 and 8. Performance-based seismic engineering: vision for an earthquake resilient society. Dordrecht: Springer; 2014. p. 315–32.
8. Kassem MM, Nazri FM, Farsangi EN. The seismic vulnerability assessment methodologies: a state-of-the-art review. Ain Shams Eng J. 2020;11(4):849–64.
9. Maio R, Tsionis G. Seismic fragility curves for the European building stock. Brussels JRC Tech Report, European Commission; 2015.
10. Shamrao PV. Seismic fragility analysis for Torsionally imbalanced Shear Wall concrete building. J Inst Eng Ser A. 2021;102(2):553–63.
11. Belletti B, Martinelli E, Michelini E, Tavano M, Vecchi F. Seismic risk assessment of existing RC frame-buildings with shear walls. Seismic behaviour and Design of Irregular and Complex Civil Structures IV. Cham: Springer; 2022. p. 273–85.
12. Belletti B, Martinelli E, Michelini E, Vecchi F. Evaluation of the seismic vulnerability of existing pre-code rc core structural systems through non-linear pushover analyses. In: Papadrakakis M, Fragiadakis M, editors. COMPDYN. Athens: Eccomas Proceedia; 2021. p. 1027–38.
13. Vuran E, Bal İE, Crowley H, Pinho R. Determination of equivalent SDOF characteristics of 3D dual RC structures. In: Proceeding of the 14th World Conf Earthquake Engineering, October 12–17, 2008, Beijing, China; 2008.
14. Di Sarno L, Pugliese F. Numerical evaluation of the seismic performance of existing reinforced concrete buildings with corroded smooth rebars. Bull Earthq Eng. 2020;18(9):4227–73.
15. Bojórquez J, Ponce S, Ruiz SE, Bojórquez E, Reyes-Salazar A, Barraza M, et al. Structural reliability of reinforced concrete buildings under earthquakes and corrosion effects. Eng Struct. 2021;237:112161.
16. Belletti B, Franceschini L, Martinelli E, Michelini E, Vecchi F. Seismic fragility assessment for an existing RC framewall dual system building with corroded bars. In: Belletti B, Coronelli D, editors. fib. CACRCS DAYS; 2021. p. 185–5.
17. Nigro F, Zinco A, Martinelli E. A practice-oriented procedure for seismic reliability assessment of RC structures affected by carbonation-induced degradation. Appl Mech. 2021;2(4):820–40.
18. AICAP. Seismic design of RC buildings - guide to the application of Eurocode 2, with reference to the Italian code DM 14.1.2008 (in Italian). Rome: Pubblicemento; 2008.
19. Faella C, Lima C, Martinelli E. Non-linear static methods for seismic fragility analysis and reliability evaluation of existing structures. In: Proceedings of the 14th World Conference on Earthquake Engineering, Beijing, China. 2008. 12–7.
20. Rossetto T, Gehl P, Minas S, Galasso C, Duffour P, Douglas J, et al. FRACAS: a capacity spectrum approach for seismic fragility assessment including record-to-record variability. Eng Struct. 2016;125:337–48.
21. Belletti B, Cerioni R, Iori I. Physical approach for reinforced-concrete (PARC) membrane elements. J Struct Eng. 2001;127(12):1412–26.
22. Belletti B, Vecchi F. Implementation of steel constitutive model including buckling in ARC_CL 2.1 crack model. In: 5th International fib Congress, Melbourne, Australia. 2018.
23. Belletti B, Vecchi F, Bandini C, Andrade C, Montero JS. Numerical evaluation of the corrosion effects in prestressed concrete beams without shear reinforcement. Struct Concr. 2020;21(5):1794–809.
24. Vecchi F, Belletti B. Capacity assessment of existing RC columns. Buildings. 2021;11(4):161.
25. Geng F, Wen Z, Xu C, Chau KT. Time-dependent seismic fragility for aging RC frame structures in the inland atmosphere environment. J Earthq Eng. 2022;1–18.
26. Toniolo G, Di Prisco M. Design of structures Vol. 2 - Reinforced concrete. Limit state design (in Italian). Zanichelli, 3rd edition; 2009.
27. Belletti B, Scolari M, Vecchi F. PARC_CL 2.0 crack model for NLFEA of reinforced concrete structures under cyclic loadings. Comput Struct. 2017;191:165–79.
28. Menegotto M. Method of analysis for cyclically loaded RC plane frames including changes in geometry and non-elastic

behavior of elements under combined normal force and bending. In: Proceedings of the IABSE Symposium on Resistance and Ultimate Deformability of Structures Acted on by Well Defined Repeated Loads. 1973. 15–22.
29. Monti G, Nuti C. Nonlinear cyclic behavior of reinforcing bars including buckling. J Struct Eng. 1992;118(12):3268–84.
30. Kashani MM, Crewe AJ, Alexander NA. Nonlinear cyclic response of corrosion-damaged reinforcing bars with the effect of buckling. Construct Build Mater. 2013;41:388–400.
31. Franceschini L, Vecchi F, Belletti B. The PARC_CL 2.1 crack model for NLFEA of reinforced concrete elements subjected to corrosion deterioration. Corros Mater Degrad. 2021;2(3):474–92.
32. Tuutti K. Corrosion of steel in concrete. Cement-och betonginst; 1982.
33. Crete D. Probabilistic performance based durability Design of Concrete Structures: statistical quantification of the variables in the limit state functions. Rep No BE 2000;95–1347.
34. IN30902I - CONTECVET. A validated user's manual for assessing the residual life of concrete structures. DG Enterp CEC, (The Man Assess Reinf Struct Affect by Reinf Corros can be seen web sites IETcc (www.ietcc.csic.es) GEOCISA (www.geocisa.es)); 2001.
35. Val DV. Deterioration of strength of RC beams due to corrosion and its influence on beam reliability. J Struct Eng. 2007;133(9):1297–306.
36. Val DV, Melchers RE. Reliability of deteriorating RC slab bridges. J Struct Eng. 1997;123(12):1638–44.
37. Chen E, Berrocal CG, Fernandez I, Löfgren I, Lundgren K. Assessment of the mechanical behaviour of reinforcement bars with localised pitting corrosion by digital image correlation. Eng Struct. 2020;219:110936.
38. Jiang C, Wu Y-F, Dai M-J. Degradation of steel-to-concrete bond due to corrosion. Construct Build Mater. 2018;158:1073–80.
39. Li D, Wei R, Li L, Guan X, Mi X. Pitting corrosion of reinforcing steel bars in chloride contaminated concrete. Construct Build Mater. 2019;199:359–68.
40. Vecchi F, Belletti B, Imperia L. Ultimate chord rotation of corroded reinforced concrete columns subjected to cyclic loading. In: Fib CACRCS DAYS 2020—capacity assessment of corroded structures on-line; 2020. 385–93.
41. UNI EN 1998-3:2005. Eurocode 8—Design of structures for earthquake resistance—Part 3: Assessment and retrofitting of buildings. Brussels: CEN; 2005.
42. Meda A, Mostosi S, Rinaldi Z, Riva P. Experimental evaluation of the corrosion influence on the cyclic behaviour of RC columns. Eng Struct. 2014;76:112–23.
43. Grünthal G. European macroseismic scale 1998. European Seismological Commission (ESC); 1998.
44. Kristiawan SA, Hapsari IR, Purwanto E, Marwahyudi M. Evaluation of damage limit state for RC frame based on FE modeling. Buildings. 2021;12(1):21.
45. FEMA. Multi-Hazard Loss Estimation Methodology, Earthquake Model, Hazus-MH 2.1, Technical Manual. Washington, DC: FEMA; 2013.
46. Crowley H, Pinho R, Bommer JJ. A probabilistic displacement-based vulnerability assessment procedure for earthquake loss estimation. Bull Earthq Eng. 2004;2(2):173–219.
47. Milutinovic Z V, Trendafiloski GS. Risk-UE an advanced approach to earthquake risk scenarios with applications to different european towns. Contract EVK4-CT-2000-00014, WP4 vulnerability Curr Build 2003;1–111.
48. Lagomarsino S, Giovinazzi S. Macroseismic and mechanical models for the vulnerability and damage assessment of current buildings. Bull Earthq Eng. 2006;4(4):415–43.
49. Fajfar P. Capacity spectrum method based on inelastic demand spectra. Earthq Eng Struct Dyn. 1999;28(9):979–93.
50. Dolšek M, Fajfar P. IN2-a simple alternative for IDA. In Paper presented at 13th World Conference on Earthquake Engineering. 2004. 1–6.
51. Smerzini C, Galasso C, Iervolino I, Paolucci R. Ground motion record selection based on broadband spectral compatibility. Earthq Spectra. 2014;30(4):1427–48.
52. Freeman SA. The capacity spectrum method as a tool for seismic design. Proceedings of the 11th European conference on earthquake engineering. France, Paris; 1998. p. 6–11.
53. Pitilakis K. Systemic seismic vulnerability and risk analysis for buildings, lifeline networks and infrastructures safety gain (SYNER-G). Deliverable D7.1—Functional Fragility Curve Archive 2009.
54. Kappos AJ, Panagopoulos G, Panagiotopoulos C, Penelis G. A hybrid method for the vulnerability assessment of R/C and URM buildings. Bull Earthq Eng. 2006;4(4):391–413.
55. Ahmad N, Crowley H, Pinho R. Analytical fragility functions for reinforced concrete and masonry buildings and buildings aggregates of Euro-Mediterranean regions—UPAV methodology. Internal Report, Syner-G Project 2009/2012; 2011.
56. Tsionis G, Papailia A, Fardis M. Analytical fragility functions for reinforced concrete buildings and buildings aggregates of Euro-Mediterranean regions—UPAT methodology. Internal Report, Syner-G Project 2009/2012; 2011.

AUTHOR BIOGRAPHIES

Elena Michelini, Assistant Professor in Structural Engineering, Department of Engineering and Architecture, University of Parma, Parco Area delle Scienze 181/A, 43124 Parma, Italy.
elena.michelini@unipr.it

Beatrice Belletti, Full Professor in Structural Engineering, Department of Engineering and Architecture, University of Parma, Parco Area delle Scienze 181/A, 43124 Parma, Italy.
beatrice.belletti@unipr.it

Lorenzo Franceschini, PhD Student, Department of Engineering and Architecture, University of Parma, Parco Area delle Scienze 181/A, 43124 Parma, Italy.
lorenzo.franceschini@unipr.it

Enzo Martinelli, Associate Professor in Structural Engineering, Department of Civil Engineering, University of Salerno, Via Giovanni Paolo II 132, 84084 Fisciano (SA), Italy.
e.martinelli@unisa.it

How to cite this article: Michelini E, Belletti B, Franceschini L, Martinelli E. Time-dependent seismic fragility curves for existing RC core-wall buildings exposed to corrosion. Structural Concrete. 2022. https://doi.org/10.1002/suco.202200373